

See discussions, stats, and author profiles for this publication at: <https://www.researchgate.net/publication/263939498>

A Series of Squaraine Dyes: Effects of Side Chain and the Number of Hydroxyl Groups on Material Properties and Photovoltaic Performance

ARTICLE in CHEMISTRY OF MATERIALS · JANUARY 2014

Impact Factor: 8.35 · DOI: 10.1021/cm4034929

CITATIONS

21

READS

38

9 AUTHORS, INCLUDING:



Hisahiro Sasabe

Yamagata University

93 PUBLICATIONS 3,120 CITATIONS

[SEE PROFILE](#)



Hiroshi Katagiri

Yamagata University

54 PUBLICATIONS 955 CITATIONS

[SEE PROFILE](#)



Xiao-Feng Wang

Jilin University

44 PUBLICATIONS 837 CITATIONS

[SEE PROFILE](#)



Ziruo Hong

University of California, Los Angeles

128 PUBLICATIONS 7,625 CITATIONS

[SEE PROFILE](#)

A Series of Squaraine Dyes: Effects of Side Chain and the Number of Hydroxyl Groups on Material Properties and Photovoltaic Performance

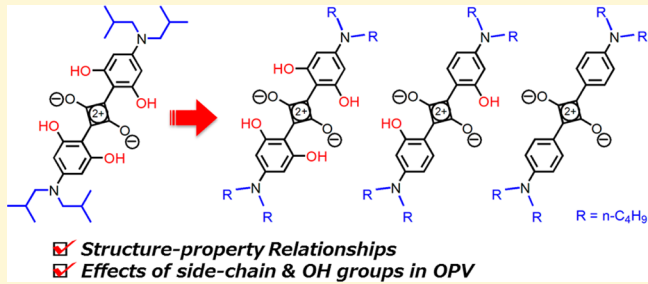
Guo Chen,[†] Hisahiro Sasabe,^{*,†} Yusuke Sasaki,[†] Hiroshi Katagiri,[†] Xiao-Feng Wang,[†] Takeshi Sano,[†] Ziruo Hong,^{*,†,‡} Yang Yang,^{*,‡} and Junji Kido^{*,†}

[†]Department of Organic Device Engineering, Graduate School of Engineering, Research Center for Organic Electronics (ROEL), Yamagata University, 4-3-16 Jonan, Yonezawa, Yamagata 992-8510, Japan

[‡]Department of Materials Science and Engineering, University of California, Los Angeles, California 90095, United States

S Supporting Information

ABSTRACT: Squaraine dyes are considered an important group of photoactive materials in the field of organic photovoltaic devices. In this work, we purposely tuned the side chains and number of hydroxyl (OH) groups in a series of squaraine (SQ) dyes, i.e., SQ1–4, to investigate the effect of structural variations on the material properties as well as the performance of these dyes as donor materials in bulk heterojunction (BHJ) photovoltaic cells. The material structure and properties of these SQs were systematically characterized using various tools. Solution-processed BHJ photovoltaic cells based on these SQ compounds combined with [6,6]-phenyl-C71-butyric acid methyl ester (PC_{71}BM) as an acceptor gave efficient power conversion efficiencies greater than 4.0% under AM 1.5G solar illumination at 100 mW/cm^2 . Our observations show that the OH groups deepened the highest occupied molecular orbital (HOMO) of the donor and thus enhanced the open-circuit voltage, whereas the linear chain improved the charge transport properties in the BHJ films. Both the side chain and the number of OH groups play important roles in determining the aggregation behavior of these SQs in solid-state films: SQ1, which contains four OH groups and branched side chains, exhibits J-aggregation because of the steric hindrance of its side chains; SQ2, which contains four OH groups and linear side chains, exhibits both H-aggregation and J-aggregation; SQ3, which contains two OH groups and linear side chains, exhibits preferential H-aggregation; SQ4, which contains linear side chains without OH groups, exhibits J-aggregation, this is most likely because of its strong intermolecular coupling and intermolecular hydrogen-bonding interactions to form a head-to-tail packing mode, i.e., J-aggregation. Interestingly, the absorption of J-aggregates in BHJ cells contributes to the cells' photoresponse at long wavelengths, and thus results in higher photocurrent. Our results demonstrate a clear relationship between the molecular structures of SQ dyes and their physical properties that govern their photovoltaic performance.



INTRODUCTION

Organic photovoltaic (OPV) cells have shown great potential as renewable energy sources because of their promising features, which include compatibility with large-area and low-cost coating techniques, lightweight, and device flexibility.^{1–4} In the past decade, the OPV field has achieved great progress in power conversion efficiency (PCE).⁵ The materials used in OPV devices—especially the electron donor and acceptor materials—govern their performance.^{6–8} Organic compounds for OPV devices should satisfy several basic requirements: (i) the materials should exhibit intense and broad absorption in the visible and near-infrared (NIR) regions for efficient light harvesting; (ii) the energy levels of the donor and acceptor materials should be matched to achieve efficient charge separation and a large open-circuit voltage (V_{oc}); (iii) the charge carriers should exhibit high mobility to facilitate efficient charge transport and extraction. Recently, small-molecule-based

OPV cells have attracted increasing attention because of their advantages, which include facile material synthesis and purification, and tunable molecular structures and energy levels.^{8–10} Squaraine (SQ) dyes have demonstrated strong potential for use in OPV cells because of their high absorption coefficients and intense absorption in the visible and NIR spectral regions. Control of the aggregation behavior of SQ molecules in solid-state films plays an important role in improving the photocurrent, and thus the PCE of the OPV cell.^{11–13}

The SQ family is a large material library suitable for light harvesting.^{14,15} Most recently, several series of SQ dyes have been introduced into OPV cells as electron donors in

Received: May 7, 2013

Revised: January 9, 2014



ACS Publications

© XXXX American Chemical Society

A

dx.doi.org/10.1021/cm4034929 | Chem. Mater. XXXX, XXX, XXX–XXX

combination with a fullerene derivative, and such cells have exhibited efficient OPV performance.^{16–19} Silvestri et al. combined SQ derivatives and [6,6]-phenyl-C61-butrylic acid methyl ester (PC_{61}BM) for use in solution-processed bulk heterojunction (BHJ) cells, and achieved a PCE of 2% with an alkenyl-functionalized SQ.¹⁶ Mayerhöffer et al. have reported a series of NIR-absorbing acceptor-substituted SQ-based BHJ cells and a PCE of 1.8% with an astonishingly high short-circuit current density (J_{sc}) of 12.6 mA/cm^2 .¹⁷ Among SQ derivatives, SQs with four hydroxyl (OH) groups show outstanding performance in OPV cells. Wei et al. have explored a series of SQ derivatives based on 2,4-bis[4-(*N,N*-dialkylamino)-2,6-dihydroxyphenyl] squaraine or 2,4-bis[4-(*N,N*-diarylamino)-2,6-dihydroxyphenyl] squaraine and reported PCEs greater than 5%.^{18,19} As shown in these examples, SQ dyes show superior performance in OPV cells because of their large absorption coefficient of greater than $2 \times 10^5 \text{ cm}^{-1}$, their relatively small band gap of $\sim 1.7 \text{ eV}$, and their deep highest occupied molecular orbital (HOMO) level of $\sim 5.3 \text{ eV}$. We have used 2,4-bis[4-(*N,N*-diisobutylamino)-2,6-dihydroxyphenyl] squaraine with a SQ(OH)_4 backbone as a donor for OPV cells, and achieved PCEs of $\sim 5\%$ from solution-processed BHJ cells²⁰ and PCEs greater than 6% from cells prepared using a vacuum coevaporation process.²¹ The elucidation of the effect of structural variations of SQ donors on the material properties and OPV performance is critical for the further exploration of the full potential of SQ donors in this application.

In this study, we investigated the effects of structural variations of SQ dyes on the material properties and OPV performance of BHJ cells. To do so, we designed and synthesized a series of SQ dyes with various chemical structures using different side chains and different numbers of OH groups (as shown in Chart 1), i.e., 2,4-bis[4-(*N,N*-diisobutylamino)-

2,6-dihydroxyphenyl] squaraine (SQ1), 2,4-bis[4-(*N,N*-dibutylamino)-2,6-dihydroxyphenyl] squaraine (SQ2), 2,4-bis[4-(*N,N*-dibutylamino)-2-dihydroxyphenyl] squaraine (SQ3), and 2,4-bis[4-(*N,N*-dibutylamino)-phenyl] squaraine (SQ4). Both SQ1 and SQ2 have four OH groups at the 2,6-position of the two phenyl rings, whereas the side chains at the 4-position of the two phenyl rings differ. SQ2–4 have the same side chain but different numbers of OH groups. On the basis of this series of SQs, we investigated the effects of their structure on their properties. We also tested these SQ dyes as donors in BHJ cells, and demonstrated that the structural modification caused dramatic changes in the solid-state properties of both neat SQ films and SQ:fullerene blend films as well as in their photovoltaic properties.

■ EXPERIMENTAL SECTION

Materials Synthesis. All chemicals and solvents were used as received. SQ1,²² SQ2,²² SQ3,²³ and SQ4²⁴ dyes were synthesized according to the procedure reported in the literature.^{22–24} Target compounds were confirmed to be analytically pure by ^1H -nuclear magnetic resonance (NMR) and elemental analysis and >99.9% pure by high-performance liquid chromatography (HPLC).

Characterization. Ultraviolet-visible (UV-vis) absorption spectra were collected using a UV-vis-NIR spectrophotometer (SHIMADZU, UV-3150). Photoluminescence (PL) spectra were measured using a FluoroMax-2 (Jobin-Yvon-Spek) luminescence spectrometer. The concentration of the solutions for UV-vis absorption and PL measurements was $1 \times 10^{-5} \text{ M}$ in chloroform. Thin films for UV-vis absorption and PL measurements were prepared by spin coating a chloroform solution onto quartz substrates.

Characterization of Electrochemical Properties. Cyclic voltammetry (CV) measurements were performed using a PC controlled Auto-Lab PSTAT10 electrochemical workstation in an N_2 -filled glovebox with oxygen and water contents of less than 5 ppm. The experiments were conducted in dichloromethane (CH_2Cl_2 ; DCM) with 0.1 M tetrabutylammonium tetrafluoroborate (TBABF₄, as supporting electrolyte) at a scan rate of 0.1 V/s using a glassy carbon electrode as the working electrode, platinum wire as the counter electrode, and a Ag/Ag^+ electrode as the reference electrode. Ferrocene was used as an internal standard. The electrochemical potential was internally calibrated against the standard ferrocene/ferrocenium (Fc/Fc^+) redox couple.

PYS Measurements. The ionization potential (I_{p}) levels of SQ1–4 as solid-state films were determined by photoemission yield spectroscopy (PYS) under vacuum ($\sim 10^{-3} \text{ Pa}$),²⁵ detailed experimental information is provided in the Supporting Information. Films with a thickness of 20 nm were prepared by spin coating the chloroform solution onto indium tin oxide (ITO) glass substrates in a N_2 -filled glovebox.

X-ray Crystallography. Green-brown needlelike single crystals of SQ1, blue-green needle-like single crystals of SQ2, and green block single crystals of both of SQ3 and SQ4 were grown by a slow evaporation of chloroform under a N_2 atmosphere. Single-crystal X-ray crystallography data were collected at 93 K on a Rigaku R-axis Rapid diffractometer equipped with a Cu-K α radiation source ($\lambda = 1.54187 \text{ \AA}$). All calculations were performed using the Crystal Structure crystallographic software package.²⁶ The structure was solved by direct methods using the program SHELXS-97, and it was refined by full-matrix least-squares methods on F^2 using SHELXL-97.²⁷

Analysis of Film Morphology. X-ray diffraction (XRD) patterns for thin films were collected using a high-resolution XRD diffractometer (SmartLab, Rigaku Co.). Atomic force microscopy (AFM) images were taken in air on a Veeco AFM using a tapping mode. The films for XRD and AFM measurements were prepared via the same process used to fabricate the devices: by spin coating SQ or SQ: PC_{71}BM solution onto 6-nm-thick MoO_3 -coated ITO glass substrates.

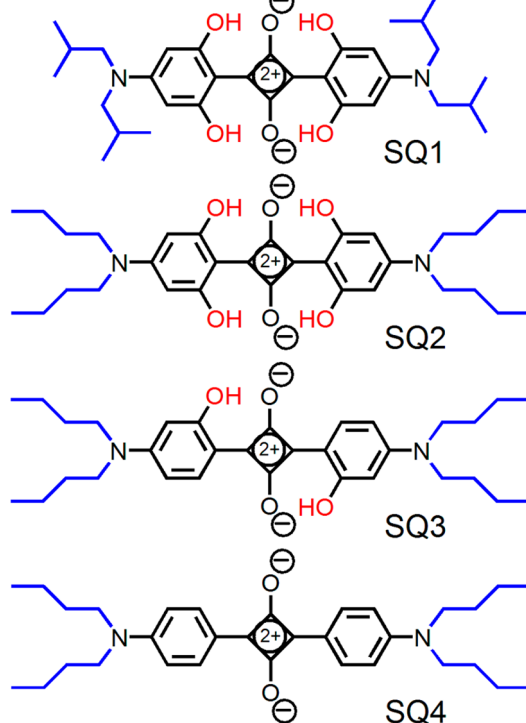


Chart 1. Molecular Structures of Squaraine (SQ) Dyes SQ1–4

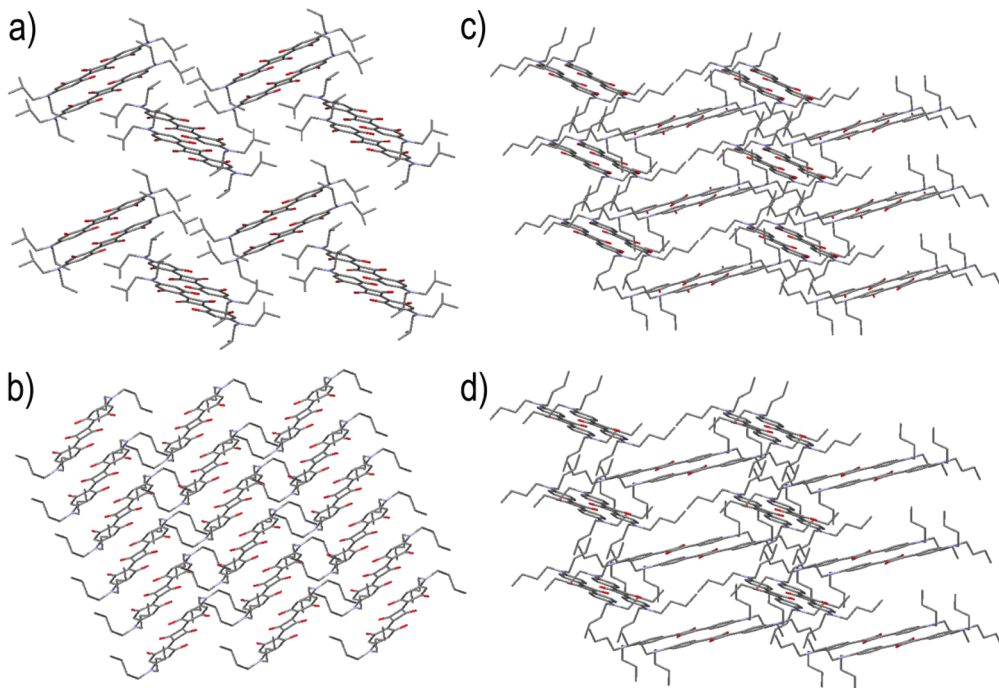


Figure 1. Molecular packing modes in single crystals of (a) SQ1, (b) SQ2, (c) SQ3, and (d) SQ4.

Characterization of Hole Mobility. Hole-only devices with a structure of ITO/MoO₃ (6 nm)/SQ (60 nm)/MoO₃ (6 nm)/Al (100 nm) were fabricated to characterize hole mobility in these SQs in neat films using the space-charge-limited current (SCLC) model.²⁸

Device Fabrication and Characterization. Patterned ITO-coated glass substrates were sequentially cleaned using detergent, deionized water, acetone, and isopropanol in an ultrasonic bath. The cleaned substrates were dried in an oven at 80 °C for 12 h before use. Substrates were exposed to UV ozone for 30 min, and were then immediately transferred into a high-vacuum chamber for the deposition of 6 nm MoO₃ at a base pressure of 1×10^{-5} Pa. Photoactive layers (thickness: 70 ± 5 nm) were fabricated by spin-coating SQ1–4:PC₇₁BM solution (the concentration of donor:acceptor blend was 20 mg/mL in chloroform) onto a MoO₃-coated ITO surface in a N₂-filled glovebox. Finally, the substrates were transferred back to the high-vacuum chamber, where BCP (10 nm) and Al (100 nm) were deposited as the top electrode, resulting in a final OPV cell with the structure ITO/MoO₃ (6 nm)/SQ:PC₇₁BM (70 nm)/BCP (10 nm)/Al (100 nm). The active area of the OPV cells was 0.09 cm², as defined by the overlap of the ITO anode and Al cathode. To obtain the average data related to device performance, two batches of devices (16 cells per batch) for each set of conditions were fabricated and tested. In addition, to characterize the carrier mobilities in the blend films using the SCLC model, hole-only and electron-only devices were also fabricated with structures of ITO/MoO₃ (6 nm)/SQ:PC₇₁BM (70 nm)/MoO₃ (6 nm)/Al (100 nm) and ITO/Cs₂CO₃ (10 nm)/SQ:PC₇₁BM (70 nm)/BCP (10 nm)/Al, respectively.²⁰ Current density–voltage (J – V) and external quantum efficiency (EQE) characterizations of OPV cells were performed on a CEP-2000 integrated system manufactured by Bunkoukeiki Co., as reported previously.^{20,21} The integration of EQE data over a AM1.5G solar spectrum yielded calculated J_{sc} values with an experimental variation of less than 3% relative to the J_{sc} measured under 100 mW/cm² simulated AM1.5G light illumination.

■ RESULTS AND DISCUSSION

Materials Design. In our previous study, we found SQ1 to exhibit promising properties such as strong NIR absorption and a deep HOMO for high-performance OPV cells.^{20,21,29} However, the low hole mobility of SQ1, which is typically on

the order of 1×10^{-5} cm²/(V s), limits the thickness of the active layer, and hence the light harvesting, J_{sc} , and fill factor (FF) in a OPV cell. We attributed the low hole mobility of SQ1 to strong steric hindrance of bulky side chains, which weakens the intermolecular π – π stacking in the core skeleton and leads to low mobility. To test our hypothesis, we used SQ2, which contains linear N-butyl groups, to reduce steric hindrance. Furthermore, to better understand the effect of OH groups on the material properties and OPV performance of SQ donors, we prepared SQ3 and SQ4 by decreasing the number of OH groups in SQ2. Thus, the four SQ compounds were divided into two groups to investigate structural effects: (1) SQ1 and SQ2, to facilitate investigation of the effects of the side chains; (2) SQ2, SQ3, and SQ4, to allow an investigation of the effects of OH groups.

Crystallography and Molecular Packing. Single-crystal structures of the SQs were analyzed to gain insight into their molecular structure and packing mode in the solid state. Table S1 (see the Supporting Information) summarizes the results of the single-crystal X-ray crystallographic analyses of SQ1–4. Notably, the results obtained for SQ1 and SQ2 are consistent with previously reported results.^{30,31} The details of X-ray crystallography results for SQ2, SQ3, and SQ4 can be viewed from the crystallographic information files (CIF files, shown in the Supporting Information). SQ1, SQ3, and SQ4 have the same monoclinic crystal system with different space groups of $P2(1)/n$, $P2_1/c$, and $P2_1/c$, respectively. SQ2 has a triclinic crystal system with space group $P\bar{1}$, therefore, the arrangement of the side chain of SQ2 differs from those of the other SQs. The molecular structures of all of these SQ dyes contain an approximately planar central π -system (see Figure S1 in the Supporting Information).

As shown in Figure 1, SQ1–4 demonstrate different molecular packing modes in their crystal lattices. SQ1 molecules exhibit edge-to- π stacking,³⁰ SQ2 molecules show closely packed π – π stacking, and SQ3 and SQ4 molecules demonstrate similar edge-to- π stacking. We believe the different

Table 1. Photophysical Properties of SQ1–4

dye	ϵ ($\times 10^5$ M $^{-1}$ cm $^{-1}$)	absorption				emission		
		solution ^a		thin film ^b		λ_{em} (nm)		
		λ_{max} (nm)	λ_{onset} (nm)	E_g^{opt} (eV) ^c	λ_{max} (nm)	λ_{onset} (nm)	E_g^{opt} (eV) ^c	solution ^a
SQ1	3.6	652	672	1.85	700	735	1.69	677
SQ2	3.4	649	670	1.85	563, 668	746	1.66	671
SQ3	3.2	648	666	1.86	533, 648	750	1.65	671
SQ4	3.4	641	660	1.88	655, 770	794	1.56	666
								775

^aAbsorption/emission spectra were measured in chloroform (1×10^{-5} M). ^bThin film was spin-coated from chloroform solution onto a quartz substrate. ^cThe optical band gap was calculated from $E_g^{\text{opt}} = 1240/\lambda_{\text{onset}}$.

molecular packing modes of SQ1 and SQ2 partially stem from the side chain effect. The bulky isobutyl groups reduce the molecular packing and enlarge the distance between adjacent π -systems. In contrast, the linear N-butyl chains allow the π -conjugated system to closely stack in parallel. We also noted that SQ2 exhibits a significantly different packing mode compared with those of SQ3 and SQ4, even though all of them have the same linear N-butyl chains. The difference could arise from the OH groups because the number of OH groups affects intra- and intermolecular C–H···O hydrogen bond interactions.^{32,33} This effect was confirmed by thin layer chromatography (TLC, silica gel) analysis. The TLC analysis using chloroform as an eluent showed that the retention factors (R_f) of these SQs decrease in the order SQ1 = SQ2 (0.83) > SQ3 (0.48) ≫ SQ4 (0.06). The R_f values reflect the degree of interaction between the SQ molecules and silica gel, which is related to the strength of the hydrogen bond interactions between a single substrate molecule and silanol. Small R_f of SQ3 and SQ4 indicate that stronger intermolecular hydrogen bonds are present in these dyes.

Apart from single-crystal characterization, we also examined the molecular packing in spin-coated SQ thin films because the later is more related to the charge transport properties in thin-film-based photovoltaic cells. Out-of-plane and in-plane XRD patterns (see Figure S2 in the Supporting Information) indicate that the SQ1 film is amorphous, whereas the SQ2, SQ3, and SQ4 films have crystalline structures. These results are consistent with the side chain effects in that the bulky side chains of the SQ1 molecule result in amorphous films and linear side chains allow the formation of crystalline structures. However, SQ2, SQ3, and SQ4 exhibit completely different properties. SQ2 exhibits both face-on and edge-on orientation, whereas SQ3 and SQ4 exhibit face-on and edge-on orientations, respectively. The different molecular orientation in the solid-state film can be ascribed to different aggregation behavior of these SQs, which were verified by both absorption and PL spectroscopy of the solid-state films, as discussed in a subsequent section.

Solubility and Photophysical Properties. The solubility of SQ compounds is critically important in the fabrication of solution-processed photovoltaic cells. We therefore tested the solubility of these materials in a few solvents commonly used for OPV fabrication processing, such as dichloromethane, chloroform, and chlorobenzene. SQ1 exhibited moderate solubility, whereas SQ2–SQ4 showed good solubility in these solvents. In chloroform, the solubilities of SQ1, SQ2, SQ3, and SQ4 are 7, 25, 26, and 28 mg/mL, respectively. Therefore, we confirmed that these materials have sufficient solubility for solution coating.

We next collected the UV–vis absorption and PL spectra of these SQ compounds both in solution and as solid-state films; the results are summarized in Table 1 and Table S2 (see the Supporting Information). The normalized UV–vis absorption spectra of the four SQs in chloroform and as thin films are shown in Figure 2. In dilute solution, all of the investigated SQs

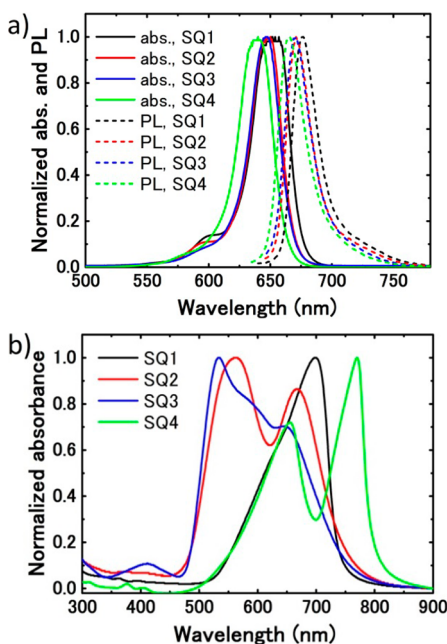


Figure 2. (a) UV–vis absorption and photoluminescence (PL) spectra of SQ1–4 in chloroform; (b) UV–vis absorption spectra of SQ1–4 as thin films on quartz substrates.

showed an intense extinction coefficient of $\epsilon = 3.2\text{--}3.6 \times 10^5$ M $^{-1}$ cm $^{-1}$ and a narrow absorption peak with $\lambda_{\text{max}} = 641\text{--}652$ nm, corresponding to monomer absorption. Compared with the absorption peaks in the spectra of samples in solution, those of neat SQ films are broadened and cover the region from 470 to 900 nm (Figure 2 and Figure S3 in the Supporting Information). The shift and broadening of the absorption bands in the spectra of the solid-state films is attributed to the aggregation of SQ molecules, which enables us to correlate the molecular structures and packing modes to the absorption properties. As mentioned in the discussion related to XRD patterns, the aggregation behavior is different in each case. For SQ1, the absorption peak exhibits a bathochromic shift from 652 nm (1.90 eV) to 700 nm (1.77 eV), with a corresponding shift in the absorption maxima of -0.13 eV (see Table S2 in the Supporting Information), which is probably due to J-aggregation.²² The branched butyl groups hinder the π – π

stacking of SQ, thereby enhancing J-aggregation instead of H-aggregation. However, linear butyl groups have much less bulk, and allow the $\pi-\pi$ stacking to form both J- and H-aggregation. Actually, both J- and H-aggregation occur in the SQ2 film, whereas only thermodynamically stable H-aggregation occurs in the SQ3 film and only J-aggregation occurs in SQ4 film.^{34–37} In the absorption spectrum of the SQ2 film, an H-aggregation band appears at 563 nm (2.20 eV) and a J-aggregation band appears at 668 nm (1.86 eV); these bands are equivalent to absorption maxima shifts of +0.29 and –0.05 eV, respectively, relative to the monomer absorption maximum at 649 nm (1.91 eV) (see Table S2 in the Supporting Information). An H-aggregation band appears at 533 nm (2.32 eV), with an absorption maximum shift of +0.41 eV relative to the absorption maximum of the monomer (see Table S2 in the Supporting Information) and the monomer absorption band at 648 nm (1.91 eV) in the absorption spectrum of the SQ3 films. In the case of the SQ4 film, an intense longer-wavelength J-aggregation band at 770 nm (1.61 eV) (absorption maximum shift: –0.32 eV relative to the monomer absorption maximum at 1.93 eV, Table S2, Supporting Information) is observed, except for the monomer absorption at 655 nm (1.89 eV). J-aggregation behavior of SQ4 is most likely due to both the stronger intermolecular charge transfer (CT) interactions between the electron-deficient central four-membered ring and the electron-rich dialkylamino phenyl groups,^{36,37} and the stronger intermolecular hydrogen bond interactions discovered using X-ray crystallography and proved by TLC analysis.

The PL spectra of these SQs in dilute solution are similar, as shown in Figure 2a, which indicates a similar origin of the PL emissions. The maximum emission peaks are located at 677, 671, 671, and 666 nm in the spectra of SQ1, SQ2, SQ3, and SQ4, respectively, and all of the peaks exhibit a full width at half-maximum of ~35 nm. The emission peaks show a 22–25-nm Stokes shift compared with the absorption spectra of these SQs in solution, corresponding to typical $S_0 \rightarrow S_1$ transitions. The solid-state films of these compounds also show dramatic difference in PL. The PL emission of SQ1 and SQ4 exhibit a very small Stokes-shift emission that peaks at 722 and 775 nm, respectively (see Figure S4 in the Supporting Information). However, SQ2 and SQ3 exhibit no detectable PL emission, which is tentatively attributed to the H-aggregation behavior of SQ2 and SQ3 in solid-state films, as mentioned in the previous paragraph.³⁴ Taking both the bathochromic-shifted absorption and the spectral narrowing of PL into consideration, we thus confirmed the J-aggregation behavior of SQ1 and SQ4 molecules in neat films.¹¹ The hypsochromic-shifted absorption and undetectable PL emission in the case of SQ2 and SQ3 neat films strongly suggest H-aggregation behavior.

Electrochemical Characterization. The electrochemical properties of these SQs were investigated using CV measurements in DCM (see Figure S5 in the Supporting Information), and the relevant data are summarized in Table 2. For the CV measurements, 0.3 mM SQ in DCM was used with 0.1 M TBABF₄ as a supporting electrolyte, and the Fc/Fc⁺ redox couple (with an absolute energy of –4.76 eV vs vacuum) was used as a reference. On the basis of the oxidation potential onset (E_{ox}) and the reduction potential onset (E_{red}) referenced to the Fc/Fc⁺ internal standard, the HOMO and lowest unoccupied molecular orbital (LUMO) were calculated according to the equations $\text{HOMO} = -(E_{\text{ox}} + 4.76)$ (eV) and $\text{LUMO} = -(E_{\text{red}} + 4.76)$ (eV), where E_{ox} and E_{red} are the oxidation potential onset and the reduction potential onset,

Table 2. Electrochemical Properties of SQ1–4 Measured Using Cyclic Voltammetry (CV) in Solution and the I_p Levels of These SQs in Solid-State Films, As Determined by Photoemission Yield Spectroscopy (PYS)

dye	E_{ox} (V) ^a	E_{red} (V) ^a	HOMO (eV)	LUMO (eV)	E_g^{ec} (eV) ^b	I_p (eV) ^c
SQ1	0.46, r	–1.30, i	–5.22	–3.46	1.76	–5.3
SQ2	0.42, r	–1.27, i	–5.18	–3.49	1.69	–5.2
SQ3	0.31, r	–1.39, i	–5.07	–3.37	1.70	–5.1
SQ4	0.26, r	–1.40, i	–5.02	–3.36	1.66	–5.2

^a $E_{\text{ox}}/E_{\text{red}}$ was determined by CV measurements in dichloromethane (CH₂Cl₂; DCM) referenced to Fc/Fc⁺ as an internal standard; r means reversible, i means irreversible. ^b E_g^{ec} (eV) = LUMO–HOMO. ^c I_p level was determined by PYS.

respectively, vs Fe/Fe⁺. The energy band gap (E_g^{ec}) was calculated according to the equation $E_g^{\text{ec}} = \text{LUMO} - \text{HOMO}$. As a result, we obtained the HOMO as –5.22, –5.18, –5.07, and –5.02 eV and the LUMO as –3.46, –3.49, –3.37, and –3.36 eV for SQ1, SQ2, SQ3, and SQ4, respectively. A comparison of the energy level of SQ2–4 reveals that the HOMO deepens as the number of OH groups increases (see Figure S6 in the Supporting Information), which suggests that the intramolecular hydrogen bonding reduces the overall energy in the SQ core via the participation of the conjugated structures. This trend is consistent with that predicted by density functional theory (DFT) calculations (see the Supporting Information). With deepened HOMO, we also expect higher V_{oc} in OPV devices, as is discussed later.

PYS Characterization. The I_p levels for the SQ1–4 films were determined using PYS measurements (see Figure S7 in the Supporting Information). Notably, the tendencies of the I_p levels of the SQ1–3 films are similar to those of the samples in solution. However, the solid-state I_p level of SQ4 is deeper than the solution-state HOMO estimated using CV measurements (see Table 2), which is attributed to the strong intermolecular CT interactions in a J-aggregated film, reducing the electron density of the HOMO in a single SQ4 molecule.^{11,17} We thus conclude that H/J-aggregation behavior not only substantially influences the absorption properties but also influences the energy levels observed in PYS. According to Kasha's molecular exciton theory,³⁸ as depicted in Figure S8 (see the Supporting Information), the dye molecule is regarded as a point dipole and the excitonic state of the dye aggregate splits into two levels through the electrostatic interaction of transition dipoles. The optical transitions from the ground state to the excited state are allowed in the upper level of the excitonic band in the case of the H-aggregate, whereas they are allowed in the lower level of the excitonic band in the case of the J-aggregate. Therefore, the resulting oxidized states (excited states formed through the removal of an electron) in the H-aggregate cases (i.e., SQ2 and SQ3) are higher than those of the J-aggregate cases (i.e., SQ1 and SQ4).

Hole Mobility. To analyze the hole mobilities of these SQs in thin films, we fabricated hole-only devices with a structure of ITO/MoO₃ (6 nm)/SQ (60 nm)/MoO₃ (6 nm)/Al (100 nm) and characterized them on the basis of the SCLC model.²⁸ The SCLC-estimated hole mobilities of SQ1, SQ2, SQ3, and SQ4 are 3.5×10^{-5} , 1.6×10^{-4} , 4.2×10^{-5} , and 1.9×10^{-4} cm²/(V s), respectively. The hole mobilities of these SQs are consistent with the XRD results for the SQ films. The higher hole

mobilities in SQ2 and SQ4 can be ascribed to the crystalline features of the SQ2 and SQ4 films.

OPV Cell Performance. To further study the effects of the side chain and the number of OH groups on the photovoltaic performance of SQ-based BHJ cells, we fabricated and characterized solution-processed BHJ cells using each SQ as a donor combined with [6,6]-phenyl-C₇₁-butyric acid methyl ester (PC₇₁BM) as an acceptor. The device structure of the BHJ cells was ITO/MoO₃ (6 nm)/SQ:PC₇₁BM (70 nm, 1: x)/BCP (10 nm)/Al (100 nm) ($x = 1\text{--}8$). The active layer SQ:PC₇₁BM was spin-coated from chloroform solution. On the basis of our previous study, we found that 70 ± 5 nm was the optimum active layer thickness in an SQ1-based BHJ system, and the blend ratio of the donor and acceptor significantly affects the carrier mobility in the photoactive layer and the OPV performance.²⁰ For comparison, we used a 70 nm thick SQ:PC₇₁BM film as the active layer in each case, and then tuned the blend ratio of SQ and PC₇₁BM from 1:1 to 1:8 to optimize the ratio with respect to device performance. The devices were characterized as shown in Figure 3 and Figures S9–S12 (see the Supporting Information); the key OPV parameters are listed in Table 3.

Figure S9 (see the Supporting Information) shows the J – V characteristics and EQE spectra of the SQ1-based BHJs with various SQ1/PC₇₁BM blend ratios. In the SQ1-based BHJ system reported in our previous study,²⁰ a 1:5 ratio between SQ1 and PC₇₁BM yielded the maximum PCE of 4.3%, with $J_{sc} = 10.8 \text{ mA/cm}^2$, $V_{oc} = 0.94 \text{ V}$, and FF = 0.43.

The variations in the J – V curves and EQE spectra with different donor/acceptor ratios in the SQ2-based BHJ system are shown in Figure S10 (Supporting Information). The optimized device with a 1:1.5 ratio delivers $J_{sc} = 9.6 \text{ mA/cm}^2$, $V_{oc} = 0.87 \text{ V}$, FF = 0.50, and PCE = 4.2%; all other ratios generated a PCE greater than 3%. As shown in Table 3, FF decreased from 0.53 to 0.39 as the blend ratio was varied from 1:1 to 1:8. This behavior is attributed to the crystalline structure in the active layer with a high SQ2 weight ratio, which led to greater carrier mobility compared with that in amorphous films with 1:3, 1:5, and 1:8 ratios (see Figure S13 and Table S3 in the Supporting Information).

In the case of SQ3-based BHJ cells (see Figure S11 in the Supporting Information), a 1:1 ratio yielded a much lower PCE compared with that achieved with other ratios, which may be due to poor charge transport.²⁰ In films prepared at ratios of 1:2, 1:3, and 1:5, the same PCE of 2.6% was obtained, with $J_{sc} = 7.8\text{--}8.3 \text{ mA/cm}^2$, $V_{oc} = 0.76\text{--}0.77 \text{ V}$, and FF = 0.41–0.43.

In the case of SQ4-based BHJs (Figure S12, Supporting Information), the optimum SQ4:PC₇₁BM ratios 1:1 and 1:1.5 yielded a PCE of 1.7%, with $J_{sc} = 5.9\text{--}6.2 \text{ mA/cm}^2$, $V_{oc} = 0.61\text{--}0.63 \text{ V}$, and FF = 0.44–0.45. Similar to the case of SQ2, crystalline SQ4:PC₇₁BM films with an active layer prepared at ratios of 1:1 and 1:1.5 (see Figure S14 in the Supporting Information) resulted in greater FFs than those of OPV cells prepared using other ratios.

Because carrier mobility is one of the key parameters that dominates the charge extraction of OPV devices, we also characterized the hole and electron mobilities in SQ:PC₇₁BM blend films using the SCLC model. The calculated mobility values from three typical SQ:PC₇₁BM blend ratios of 1:1, 1:1.5, and 1:5 are summarized in Table S3 (see the Supporting Information). When the SQ donors are blended with PC₇₁BM acceptors, the hole mobility of the resulting films decreases and their electron mobility increases as the amount of PC₇₁BM is

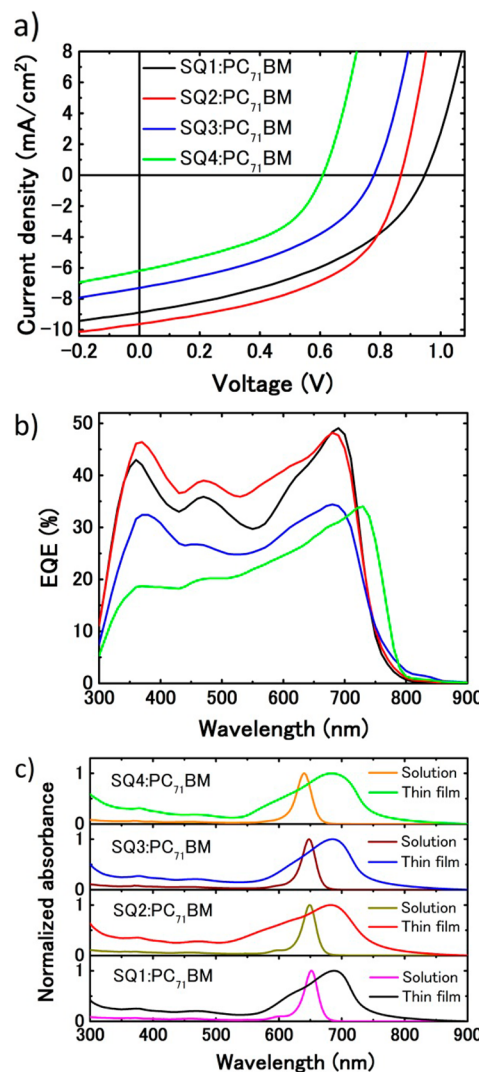


Figure 3. (a) J – V characteristics illuminated under AM 1.5 G solar spectrum at 100 mW/cm^2 illumination; (b) EQE spectra of SQ1–4-based bulk heterojunction (BHJ) cells with a donor:acceptor ratio of 1:1.5; (c) UV–vis absorption spectra of the SQ:PC₇₁BM (1:1.5) blends in solution ($1 \times 10^{-5} \text{ M}$) and as solid-state films.

increased. The balanced hole and electron mobilities in devices based on SQ2 and SQ4 films with a SQ:C₇₁BM ratio of 1:1.5 led to the most efficient charge extraction, thus, to optimized device performance. In contrast, the unbalanced hole and electron mobilities in SQ3/PC₇₁BM (1:1.5) devices resulted in poor charge transport properties, which may explain the diminished device performance and smaller photoresponse in the EQE spectrum of these devices compared with those of SQ1- and SQ2-based devices (Figure 3b).

The molecular packing of SQ compounds in the blend films is disturbed by the existence of PC₇₁BM. Yet, we observed a trend similar to that observed in the neat films. To understand the OPV performance of different SQ-based BHJ cells, we used AFM and XRD measurements to investigate the film morphology of the OPV active layer, i.e., SQ:PC₇₁BM, and in each case, chose films with a 1:1.5 donor-to-acceptor ratio for comparison (Figure 4 and Figures S14 and S15 in the Supporting Information). A high root-mean-square (RMS) roughness of 2.8 nm for the SQ2:PC₇₁BM film and 6.4 nm for the SQ4:PC₇₁BM film, as determined from AFM images and

Table 3. Summary of the Key Parameters in SQ1–4-Based BHJ Cells with Various Donor–Acceptor Blend Ratios

OPV cell	weight ratio	J_{sc} (mA/cm ²)	V_{oc} (V)	FF	PCE (%)
SQ1-based BHJs	1:1	5.0(±0.1)	0.95(±0.01)	0.31(±0.02)	1.4(±0.2)
	1:1.5	8.7(±0.2)	0.94(±0.01)	0.41(±0.02)	3.4(±0.2)
	1:2	9.2(±0.2)	0.92(±0.01)	0.41(±0.02)	3.4(±0.3)
	1:3	9.8(±0.2)	0.93(±0.01)	0.41(±0.02)	3.7(±0.3)
	1:5	10.6(±0.2)	0.93(±0.01)	0.41(±0.02)	4.0(±0.3)
	1:8	8.9(±0.2)	0.92(±0.01)	0.37(±0.02)	3.0(±0.3)
SQ2-based BHJs	1:1	7.9(±0.1)	0.86(±0.01)	0.52(±0.01)	3.4(±0.2)
	1:1.5	9.4(±0.2)	0.86(±0.01)	0.49(±0.01)	4.0(±0.2)
	1:2	9.3(±0.2)	0.83(±0.01)	0.48(±0.01)	3.7(±0.2)
	1:3	9.7(±0.2)	0.82(±0.01)	0.39(±0.02)	3.1(±0.3)
	1:5	9.4(±0.2)	0.83(±0.01)	0.40(±0.02)	3.1(±0.3)
	1:8	9.5(±0.2)	0.83(±0.01)	0.37(±0.02)	2.9(±0.3)
SQ3-based BHJs	1:1	4.8(±0.1)	0.78(±0.01)	0.38(±0.02)	1.3(±0.2)
	1:1.5	7.1(±0.2)	0.77(±0.01)	0.40(±0.02)	2.2(±0.2)
	1:2	7.6(±0.2)	0.76(±0.01)	0.41(±0.02)	2.3(±0.3)
	1:3	8.1(±0.2)	0.75(±0.01)	0.39(±0.02)	2.3(±0.3)
	1:5	8.1(±0.2)	0.75(±0.01)	0.39(±0.02)	2.3(±0.3)
	1:8	7.1(±0.2)	0.78(±0.01)	0.37(±0.02)	2.0(±0.2)
SQ4-based BHJs	1:1	5.8(±0.1)	0.62(±0.01)	0.44(±0.01)	1.5(±0.2)
	1:1.5	6.1(±0.1)	0.60(±0.01)	0.43(±0.01)	1.5(±0.2)
	1:2	5.3(±0.1)	0.60(±0.01)	0.35(±0.02)	1.0(±0.2)
	1:3	5.4(±0.1)	0.59(±0.01)	0.35(±0.02)	1.1(±0.2)
	1:5	5.4(±0.1)	0.60(±0.01)	0.37(±0.02)	1.1(±0.2)
	1:8	5.0(±0.1)	0.59(±0.01)	0.37(±0.02)	1.0(±0.2)

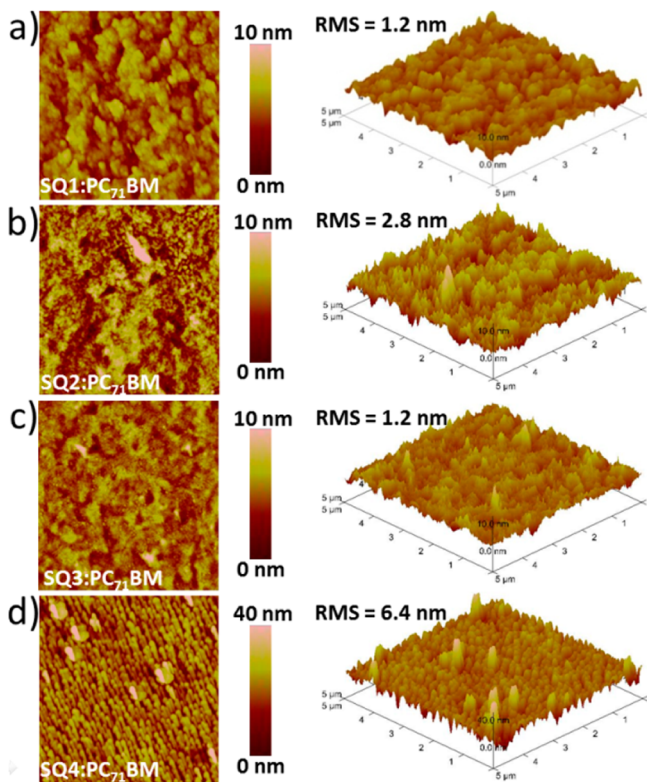


Figure 4. Atomic force microscopy (AFM) topographic and 3D images of (a) SQ1:PC₇₁BM (1:1.5), (b) SQ2:PC₇₁BM (1:1.5), (c) SQ3:PC₇₁BM (1:1.5), and (d) SQ4:PC₇₁BM (1:1.5) films spin-coated onto MoO₃-coated indium tin oxide (ITO) glass substrates.

clear peaks in the XRD patterns, indicate that the SQ2:PC₇₁BM and SQ4:PC₇₁BM films with a 1:1.5 ratio are crystalline, whereas the SQ1- and SQ3-based blend films are amorphous.

The crystalline features of the SQ2:PC₇₁BM and SQ4:PC₇₁BM films contribute to their higher carrier mobility (see Table S3 in the Supporting Information), and thus to their higher FF in related BHJ cells. In addition, out-of-plane and in-plane XRD patterns of the SQ:PC₇₁BM (1:1.5) films (see Figures S13–S15 in the Supporting Information) indicate that SQ2 and SQ4 crystallites exhibit face-on and edge-on orientations in blend films, respectively. The molecular orientation of a film is well-known to substantially affect its photovoltaic properties,³⁹ thus, the face-on orientation facilitates charge transport and results in a higher PCE than that achieved in the case of edge-on orientation. The edge-on orientation of SQ4 molecules in the blend film, and thus its poorer charge transport properties, is a possible reason for its lower photoresponse compared with those of other SQ cases, as indicated by their EQE spectra (Figure 3b).

A comparison of the OPV performance of different SQ-based BHJ devices (Figures 3 and 5 and Table 3) reveals a clear relationship among the molecular structure, material properties, and OPV performance of these SQ compounds, as summarized in Table S4 (see the Supporting Information): (i) As shown in Figures 3a and 5a, SQ2- and SQ4-based devices with a SQ:PC₇₁BM ratio of 1:1.5 show higher FFs than other SQ cases, which is attributed to the higher charge transport efficiency that results from the greater hole mobility in SQ2- and SQ4-based blend films compared with those in other SQ cases. The higher mobility is due to the crystalline features of SQ2 and SQ4 in blended films. (ii) V_{oc} of these SQ-based devices decrease in the order SQ1 > SQ2 > SQ3 > SQ4 (Figures 3b and 5b); this trend is consistent with HOMO of these SQs. In BHJ OPV cells, V_{oc} depends primarily on the difference between the HOMO of the donor and the LUMO of the acceptor; i.e., a deeper HOMO results in a higher V_{oc} of the OPV cell.⁸ The number of OH groups strongly influences the HOMO of SQ dyes, and thus V_{oc} of OPV cells. On the other

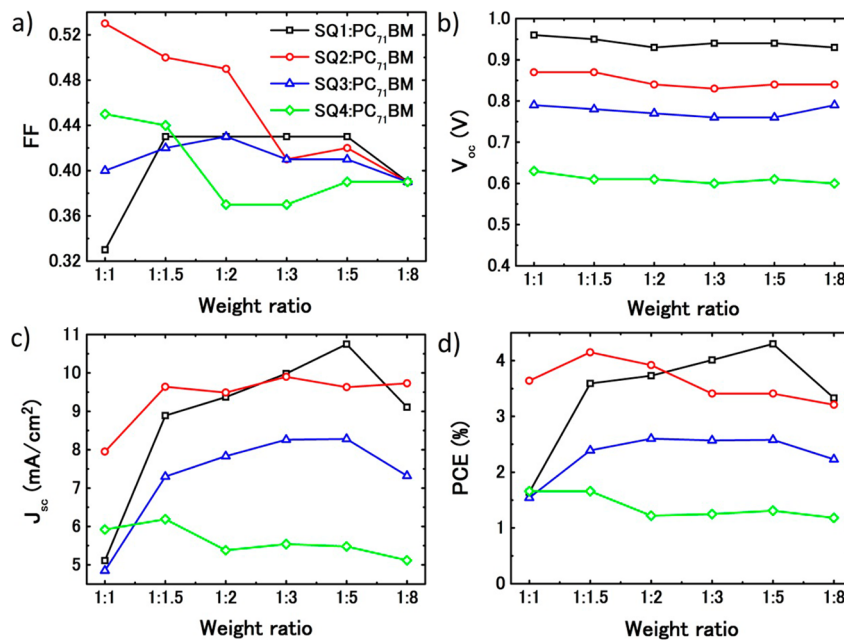


Figure 5. Photovoltaic characteristics of SQ1–4-based BHJ cells with various donor–acceptor blend ratios under a AM 1.5 G solar spectrum at 100-mW/cm² illumination: (a) FF, (b) V_{oc} , (c) J_{sc} , and (d) PCE as functions of the blend ratio.

hand, the V_{oc} can be sensitive to the orientations of the donor and acceptor molecules, which also stems from the side chain effects.⁴⁰ (iii) Because of the low hole mobilities in the SQ1- and SQ3-based devices, the J_{sc} and PCE of these devices are maximized at a 1:5 donor:acceptor ratio (Figures 3c, d); in contrast, the OPV performance of SQ2- and SQ4-based devices is maximized at a 1:1.5 ratio primarily because the aggregation of donor molecules enhances carrier mobilities. (iv) The absorption bands of SQ dyes in SQ:PC₇₁BM films are broadened, and they exhibit a 33–44 nm bathochromic shift compared with those of SQ dyes in SQ:PC₇₁BM solutions (Figure 3c), which indicates that all of the investigated SQs exhibit obvious J-aggregation behavior in the SQ:PC₇₁BM active layers. The J-aggregation contributes to the absorption of longer wavelengths, which result in higher J_{sc} and thus greater PCE in BHJ cells.^{11–13}

CONCLUSIONS

A series of SQ dyes have been used to investigate the effects of the side chains and the number of OH groups on material properties and photovoltaic performance. Although these SQs exhibit very small structural differences, they differ substantially in their molecular packing, material properties, and OPV performance. Single-crystal X-ray crystallography and XRD results revealed that the material properties are closely related to the molecular structures of these SQs. Solution-processed BHJ cells prepared using these SQ compounds as donors combined with PC₇₁BM as an acceptor were determined to provide efficient power conversion efficiencies (PCEs) of greater than 4.0% under AM 1.5G solar illumination at 100 mW/cm². Our investigations indicated that both the side chain and the number of OH groups play important roles in determining the aggregation behavior in neat films. These SQ dyes with different side chains and different numbers of OH groups exhibit substantially different aggregation behavior in SQ films, which results in dramatically different molecular orientations in the films, and thus, different photophysical

properties and hole mobilities. Interestingly, all of the investigated SQs exhibit J-aggregation in a SQ:PC₇₁BM active layer. The absorption of the J-aggregates improves both the photoresponse at longer wavelengths and thus higher J_{sc} in OPV cells that contain these active layers. In addition, the number of OH groups controls the HOMO level of these SQ dyes through intramolecular hydrogen bonding interactions. The SQs with four OH groups possess deeper HOMO levels, and thus provide higher V_{oc} in OPV devices. These results demonstrate a clear relationship between the molecular structures of the SQ dyes and their physical properties that govern their photovoltaic performance. Our findings provide fundamental guidance for designing novel SQ derivatives for high-performance OPV cells.

ASSOCIATED CONTENT

S Supporting Information

Crystallographic information files (CIFs) of SQ2 (CCDC 958817), SQ3 (CCDC 936579), and SQ4 (CCDC 936697) compounds; molecular packing in crystals, DFT calculations, thermal properties of SQ1–4, and a detailed discussion of the SQ1–4-based BHJ cells; UV-vis absorption spectra of each SQ in solution and thin film, XRD patterns of neat SQ and blended SQ:PC₇₁BM films, CV curves of all SQs in solution, PYS spectra of each SQ in a solid-state film, J – V curves and EQE spectra of SQ1–4-based BHJ cells, and absorption spectra of the blended SQ:PC₇₁BM films. This material is available free of charge via the Internet at <http://pubs.acs.org>.

AUTHOR INFORMATION

Corresponding Authors

- *E-mail: h-sasabe@yz.yamagata-u.ac.jp.
- *E-mail: zhong@ucla.edu
- *E-mail: yangy@ucla.edu
- *E-mail: kid@yz.yamagata-u.ac.jp

Notes

The authors declare no competing financial interest.

ACKNOWLEDGMENTS

We thank the Japan Science and Technology Agency (JST) for financial support via the Japan Regional Innovation Strategy Program by the Excellence (J-RISE) and the Adaptable and Seamless Technology Transfer Program (A-STEP, AS232Z00929D and AS251Z00216M). Moreover, the authors are grateful to thank Dr. K. Nakayama, Dr. D. Yokoyama, Dr. J. Hu, Ms. H. Nakanishi, Mr. Y. Watanabe, Mr. S. Mizoi, and Mr. Y. Ueno for their technical assistance and scientific discussions.

REFERENCES

- (1) Tang, C. W. *Appl. Phys. Lett.* **1986**, *48*, 183.
- (2) Günes, S.; Neugebauer, H.; Sariciftci, N. S. *Chem. Rev.* **2007**, *107*, 1324.
- (3) Ameri, T.; Khoram, P.; Min, J.; Brabec, C. J. *Adv. Mater.* **2013**, *25*, 4245.
- (4) Li, G.; Zhu, R.; Yang, Y. *Nat. Photonics* **2012**, *6*, 153.
- (5) You, J.; Dou, L.; Yoshimura, K.; Kato, T.; Ohya, K.; Moriarty, T.; Emery, K.; Chen, C. C.; Gao, J.; Li, G.; Yang, Y. *Nat. Commun.* **2013**, *4*, 1446.
- (6) Arias, A. C.; MacKenzie, J. D.; McCulloch, I.; Rivnay, J.; Salleo, A. *Chem. Rev.* **2010**, *110*, 3.
- (7) Dennler, G.; Scharber, M. C.; Brabec, C. J. *Adv. Mater.* **2009**, *21*, 1323.
- (8) Mishra, A.; Bäuerle, P. *Angew. Chem., Int. Ed.* **2012**, *51*, 2020.
- (9) Lin, Y.; Li, Y.; Zhan, X. *Chem. Soc. Rev.* **2012**, *41*, 4245.
- (10) Zhou, J.; Wan, X.; Liu, Y.; Zuo, Y.; Li, Z.; He, G.; Long, G.; Ni, W.; Li, C.; Su, X.; Chen, Y. *J. Am. Chem. Soc.* **2012**, *134*, 16345.
- (11) Chen, G.; Sasabe, H.; Lu, W.; Wang, X.; Kido, J.; Hong, Z.; Yang, Y. *J. Mater. Chem. C* **2013**, *1*, 6547.
- (12) Spencer, S.; Hu, H.; Li, Q.; Ahn, H. Y.; Qaddoura, M.; Yao, S.; Ioannidis, A.; Belfield, K.; Collison, C. J. *Prog. Photovolt: Res. Appl.* **2012**, DOI: 10.1002/pip.2289.
- (13) Deing, K. C.; Mayerhöffer, U.; Würthner, F.; Meerholz, K. *Phys. Chem. Chem. Phys.* **2012**, *14*, 8328.
- (14) Sreejith, S.; Carol, P.; Chithra, P.; Ajayaghosh, A. *J. Mater. Chem.* **2008**, *18*, 264.
- (15) Walker, B.; Kim, C.; Nguyen, T. Q. *Chem. Mater.* **2011**, *23*, 470.
- (16) Silvestri, F.; Irwin, M. D.; Beverina, L.; Facchetti, A.; Pagani, G. A.; Marks, T. J. *J. Am. Chem. Soc.* **2008**, *130*, 17640.
- (17) Mayerhöffer, U.; Deing, K.; Grub, K.; Braunschweig, H.; Meerholz, K.; Würthner, F. *Angew. Chem., Int. Ed.* **2009**, *48*, 8776.
- (18) Wei, G.; Wang, S.; Sun, K.; Thompson, M. E.; Forrest, S. R. *Adv. Energy Mater.* **2011**, *1*, 184.
- (19) Wei, G.; Xiao, X.; Wang, S.; Sun, K.; Bergemann, K. J.; Thompson, M. E.; Forrest, S. R. *ACS Nano* **2012**, *6*, 972.
- (20) Chen, G.; Sasabe, H.; Wang, Z.; Wang, X.; Hong, Z.; Kido, J.; Yang, Y. *Phys. Chem. Chem. Phys.* **2012**, *14*, 14661.
- (21) Chen, G.; Sasabe, H.; Wang, Z.; Wang, X. F.; Hong, Z.; Yang, Y.; Kido, J. *Adv. Mater.* **2012**, *24*, 2768.
- (22) Tian, M.; Furuki, M.; Iwasa, I.; Sato, Y.; Pu, L. S.; Tatsuura, S. J. *Phys. Chem. B* **2002**, *106*, 4370.
- (23) Kazmaier, P. M.; Hamer, G. K.; Burt, R. A. *Can. J. Chem.* **1990**, *68*, 530.
- (24) Law, K. Y.; Bailey, F. C.; Bluett, L. J. *Can. J. Chem.* **1986**, *64*, 1607.
- (25) Ishii, H.; Tsunami, D.; Suenaga, T.; Sato, N.; Kimura, Y.; Niwano, M. *J. Surf. Sci. Soc. Jpn.* **2007**, *28*, 264.
- (26) CrystalStructure, version 3.6.0;Rigaku/MSC: The Woodlands, TX, 2003.
- (27) Sheldrick, G. M. *Acta Crystallogr., Sect. A* **2008**, *64*, 112.
- (28) Shrotriya, V.; Li, G.; Yao, Y.; Chu, C. W.; Yang, Y. *Appl. Phys. Lett.* **2006**, *88*, 073508.
- (29) Chen, G.; Yokoyama, D.; Sasabe, H.; Hong, Z.; Yang, Y.; Kido, J. *Appl. Phys. Lett.* **2012**, *101*, 083904.
- (30) Wang, S.; Hall, L.; Diev, V. V.; Haiges, R.; Wei, G.; Xiao, X.; Djurovich, P. I.; Forrest, S. R.; Thompson, M. E. *Chem. Mater.* **2011**, *23*, 4789.
- (31) Dirk, C. W.; Herndon, W. C.; Cervantes-Lee, F.; Selna, H.; Martinez, S.; Kalamegham, P.; Tan, A.; Campos, G.; Velez, M.; Zyss, J.; Ledoux, I.; Cheng, L. T. *J. Am. Chem. Soc.* **1995**, *117*, 2214.
- (32) Lynch, D. E.; Byriel, K. A. *Cryst. Eng.* **1999**, *2*, 225.
- (33) Hamilton, D. G.; Lynch, D. E.; Smith, G. *Aust. J. Chem.* **1996**, *49*, 1339.
- (34) Würthner, F.; Kaiser, T. E.; Saha-Möller, C. R. *Angew. Chem., Int. Ed.* **2011**, *50*, 3376.
- (35) Dimitriev, O. P.; Dimitrieva, A. P.; Tolmachev, A. I.; Kurdyukov, V. V. *J. Phys. Chem. B* **2005**, *109*, 4561.
- (36) Wojtyk, J.; McKerrow, A.; Kazmaier, P.; Buncel, E. *Can. J. Chem.* **1999**, *77*, 903.
- (37) Law, K. Y. *J. Phys. Chem.* **1988**, *92*, 4226.
- (38) (a) Kasha, M.; Rawls, H. R.; El-Bayoumi, A. *Pure Appl. Chem.* **1965**, *11*, 371. (b) McRae, E. G.; Kasha, M. *J. Chem. Phys.* **1958**, *28*, 721.
- (39) Rand, B. P.; Cheyns, D.; Vasseur, K.; Giebink, N. C.; Mothy, S.; Yi, Y.; Coropceanu, V.; Beljonne, D.; Cornil, J.; Brédas, J. L.; Genoe, J. *Adv. Funct. Mater.* **2012**, *22*, 2987.
- (40) Lam, S. L.; Liu, X.; Zhao, F.; Lee, C. K.; Kwan, W. L. *Chem. Commun.* **2013**, *49*, 4543.